

Proposed low-energy model Hamiltonian for the spin-gapped system CuTe_2O_5

Hena Das¹, Tanusri Saha-Dasgupta¹, Claudius Gros² and Roser Valentí²

¹ *Department of Material Sciences, S. N. Bose National Center
for Basic Sciences, JD-III, Salt Lake City, Kolkata 700 098, India*

² *Institut für Theoretische Physik, Universität Frankfurt, D-60438 Frankfurt, Germany*

(Dated: September 25, 2018)

Using first-principles electronic structure calculations based on the N^{th} order muffin tin orbital (NMTO)-downfolding technique, we derived the low-energy spin model for CuTe_2O_5 . Our study reveals that this compound is a 2D coupled spin-dimer system with the strongest Cu-Cu interaction mediated by two O-Te-O bridges. We checked the goodness of our model by computing the magnetic susceptibility with the Quantum Monte Carlo technique and by comparing it with available experimental data. We also present magnetization and specific heat results which may be compared with future experimental investigations. Our derived model is in disagreement with a recently proposed model for this compound [J. Deisenhofer *et al*, Phys. Rev. B, **74** (2006) 174421]. The situation needs to be settled in terms of further experimental investigations.

PACS numbers: 75.10.Jm, 75.30.Et, 71.20.-b

I. INTRODUCTION

Significant amount of effort both experimental and theoretical has been devoted in the last years to the investigation of the behavior of low-dimensional quantum spin systems¹. A crucial piece of information needed in the process of understanding these systems is the connection between the underlying chemical complexity of the compound and the spin lattice. Often, this relation is not obvious from structural considerations and one needs to rely on *ab initio* based calculations as we will show in the present work.

Recently, in an attempt to analyze the effect of lone-pair cations like Se^{4+} or Te^{4+} on the magnetic dimensionality of Cu^{2+} -based systems, the magnetic properties of CuTe_2O_5 were investigated². CuTe_2O_5 is structurally a Cu(II)-dimer system separated by Te ions. Magnetic susceptibility measurements show a maximum at $T_{max}=56.5\text{K}$ with an exponential drop at lower temperatures signaling the opening of a spin gap. The behavior at high temperatures follows the Curie law with a Curie-Weiss temperature of $\theta=-41\text{K}^1$, what indicates that the dominant interactions in this system are antiferromagnetic. Electron spin resonance (ESR) observations suggest though that the structural dimers of CuTe_2O_5 do not coincide with the magnetic dimers². Fitting the susceptibility data to different models, such as a pure dimer model, the alternating spin-chain model and the modified Bleaney-Bowers model, show equally good agreement of the experimental data². A detailed investigation of the magnetic exchange paths using the extended Huckel tight binding (EHTB) method suggests that (i) the strongest interaction is between Cu ions which are 6th nearest neighbors (J_6) and is of antiferromagnetic super-superexchange (SSE) type mediated by a O-Te-O bridge and (ii) that the next strongest interaction is of antiferromagnetic superexchange (SE) type within the structural dimer (J_1), yielding a ratio $J_1/J_6=0.59^2$. Based on these findings, the authors of Ref. 2 proposed an alter-

nating spin chain model as the simplest possible model for CuTe_2O_5 .

Given the existence of many possible Cu-Cu interaction paths in this material whose relative importance may not be necessarily captured in EHTB study, we performed *ab initio* density functional theory (DFT) calculations and applied the NMTO-downfolding technique³. This technique has proven to be very successful in deriving the underlying spin model of a large number of low-dimensional quantum spin systems including cuprates^{4,5}, vanadates⁶ and titanates⁷. Our calculations reveal that the strongest Cu-Cu interaction in CuTe_2O_5 is the one between 4th nearest neighbor mediated by two O-Te-O bridges (J_4) followed by the interaction mediated by a single O-Te-O bridge (J_6). This is in contrast with the fact that J_6 was found in Ref. 2 to be the strongest interaction. We also obtain that the Cu-Cu interaction within the structural dimer unit (J_1) is rather weak as opposed to the findings of the EHTB study. The underlying spin model for CuTe_2O_5 derived out of our calculations is therefore different from that suggested in Ref. 2. We have also computed the magnetic susceptibility for the proposed model by performing Quantum Monte Carlo (QMC) simulations (stochastic series expansion^{8,9,10}). Our results show good agreement with the experimental observations. In view of the fact that the magnetic susceptibility is often found to be an insensitive quantity to the details of the magnetic structure, we have also calculated temperature and magnetic field dependent magnetization as well as the specific heat as a function of temperature. These results need to be tested in terms of further experimental investigations to resolve the underlying microscopic model for CuTe_2O_5 completely.

The paper is organized as follows: in section II and III we present respectively the crystal structure and the *ab initio* DFT electronic structure of CuTe_2O_5 . In section IV we discuss the effective model Hamiltonian obtained with the NMTO downfolding method. QMC results for

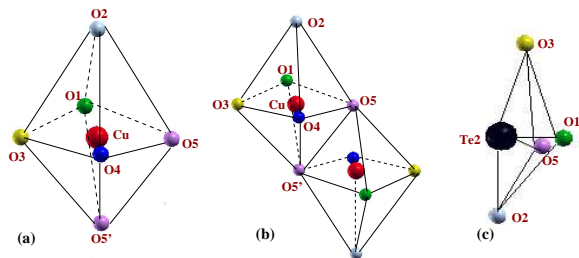


FIG. 1: (Color online) Building units of CuTe_2O_5 . (a) CuO_6 -distorted octahedron. (b) Cu_2O_{10} -structural dimer unit. (c) TeO_4 -tetrahedra.

magnetic susceptibility, magnetization and specific heat are described in section V and finally in section VI we present our conclusions.

II. CRYSTAL STRUCTURE

CuTe_2O_5 crystallizes in the monoclinic space group $P21/c^{11}$ with lattice parameters $a=6.871$ Å, $b=9.322$ Å, $c=7.602$ Å, and $\beta=109.08^\circ$. It is built out of CuO_6 distorted octahedra (Fig. 1a), with six inequivalent oxygen O1, O2, O3, O4, O5, O5' surrounding each Cu(II) ion. Each CuO_6 octahedron is elongated along the O2-O5' axis, with distances $d_{\text{Cu-O5}'}=2.303$ Å and $d_{\text{Cu-O2}}=2.779$ Å. The Cu-O distances in the CuO_4 plane range from $d_{\text{Cu-O5}}=1.948$ Å to $d_{\text{Cu-O3}}=1.969$ Å. Two neighboring CuO_6 octahedra share an edge to form a Cu_2O_{10} structural dimer (Fig. 1b). The oxygen octahedra of two Cu(II) ions within a given structural dimer are rotated by 180° with respect to each other.

The structural dimers form a chain-like structure running almost parallel to the crystallographic c axis. These chains pile along the crystallographic b axis (Fig. 2). The Te1 atoms are situated between two successive Cu(II)-structural dimer chains, while the Te2 atoms are located in between two Cu_2O_{10} structural dimers along a given chain. The local oxygen environment of the Te atoms form a TeO_4 tetrahedra (Fig. 1c). The layers containing these chains in the bc plane are stacked approximately along the crystallographic a axis with hardly any connection between the layers.

III. ELECTRONIC STRUCTURE

In order to analyze the electronic behavior of CuTe_2O_5 we carried out DFT calculations within the local density approximation by employing both the Wien2k code based on the full-potential linearized augmented plane wave (LAPW) method¹² and the Stuttgart TBLMTO-47 code based on the linear muffin-tin orbital (LMTO) method¹³. The calculated bandstructures agree well with

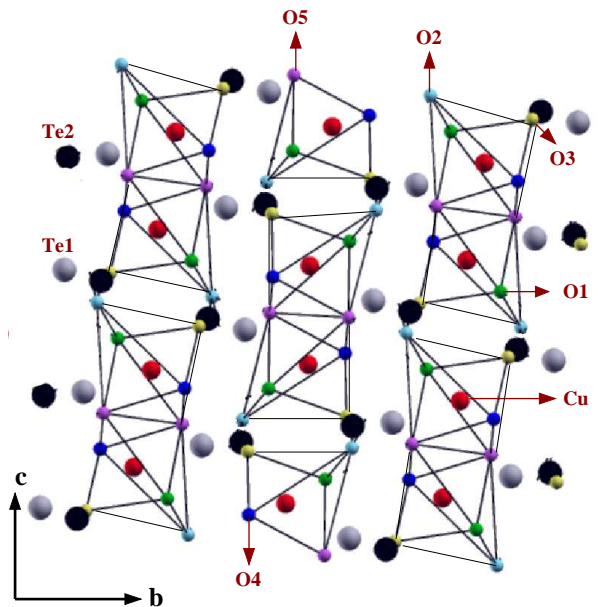


FIG. 2: (Color online) Crystal structure of CuTe_2O_5 . The largest balls represent Te1 and Te2. Te1 and Te2 are shown in grey and black colors respectively. Cu atoms are represented by medium sized balls, situated at the centre of the distorted octahedra. The smallest balls denote the oxygen atoms.

each other within the allowed error bars of the various approximations involved in these two methods. Fig. 3 and Fig. 4 show the non-spin polarized band structures and density of states (DOS) respectively of CuTe_2O_5 . The orbital contributions to the valence and conduction bands in the band structure and the DOS were determined by defining the local reference frame with the local z -axis pointing along Cu-O2 bond and the local y -axis pointing almost parallel to the Cu-O5 bond.

The predominant feature of the band structure is the isolated manifold of four bands crossing the Fermi level (E_f), formed by Cu- $d_{x^2-y^2}$ orbitals corresponding to the four Cu atoms in the unit cell, admixed with O- p states. These bands are half filled and separated from the low lying O- p and non- $d_{x^2-y^2}$ Cu valence bands by a gap of about 0.8 eV and from the Te- p -dominated high lying conduction bands by a gap of about 2.2 eV, with the zero of energy set at the LDA Fermi level. We note that in the low energy scale, the LDA results lead to a metallic state. Introduction of missing correlation effects beyond LDA, for instance with the LDA+U functional, is expected to drive the system insulating, as our LDA+U calculations corroborated.

The valence band shows Cu d_{xy} , d_{yz} , d_{zx} and $d_{3z^2-r^2}$ character dominated bands in the energy range between -2.2 eV and -1.2 eV while the O- p -dominated bands are in the energy range between -4 eV and -1.2 eV. The contribution of O2 character in the conduction bands crossing the Fermi level is found to be small compared to other oxygen because of the large Cu-O2 bond length. The Te1- p and Te2- p states show a non-negligible contribution

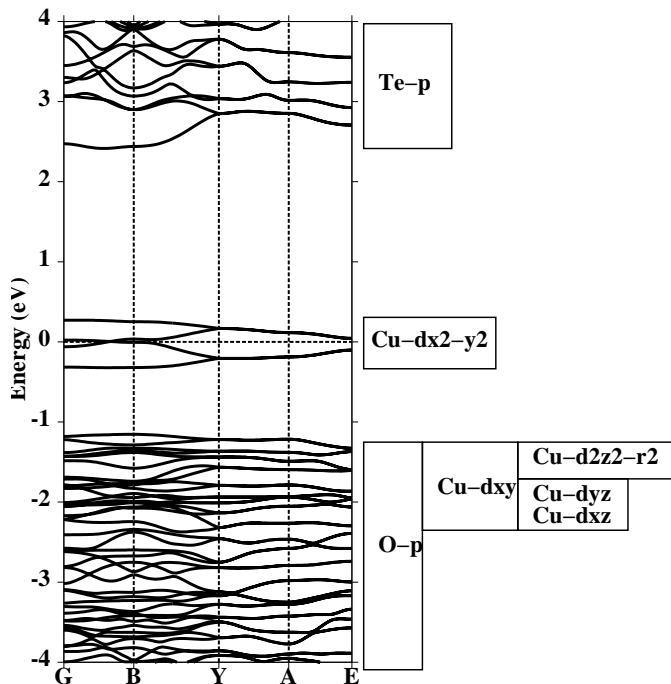


FIG. 3: LDA band structure of CuTe_2O_5 plotted along various symmetry directions of the monoclinic lattice. The zero of the energy has been set up at the LDA Fermi energy. The dominant orbital contributions in various energy ranges are shown in boxes on the right-hand side. The various Cu- d characters are shown in the local reference frame as described in the text.

to the bands crossing the Fermi energy, as pictured in the inset of Fig. 4 and play an important role in mediating the Cu-Cu exchange interaction as will be demonstrated in what follows.

IV. LOW ENERGY HAMILTONIAN - EFFECTIVE MODEL

A powerful technique to construct a low-energy, tight binding (TB) Hamiltonian starting from a LDA band structure, is given by the NMTO downfolding method³. This method derives a low-energy Hamiltonian by an energy selective, downfolding process that integrates out the high energy degrees of freedom. The low energy Hamiltonian is then defined in the basis of effective orbitals constructed via the integration out process. This process takes into account the proper renormalization effect from the orbitals that are being downfolded. The accuracy of such process can be tuned by the choice of the number of energy points (N), used for the selection of downfolded bands. If the low-energy bands form an isolated set of bands, as is the case under discussion, the constructed effective orbitals, the NMTOs, span the Hilbert space of Wannier functions or in other words, the effective orbitals are the Wannier functions correspond-

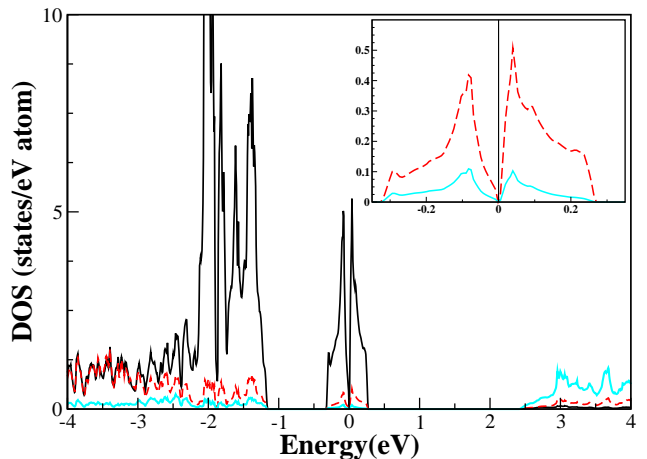


FIG. 4: (Color online) Partial density of states of Cu- d (in black full lines), O- p (in red dashed lines) and Te- p (in cyan or gray full lines) orbitals, for CuTe_2O_5 . The inset shows the density of states for O- p and Te- p in the energy range close to E_f , dominated by Cu- $d_{x^2-y^2}$ character.

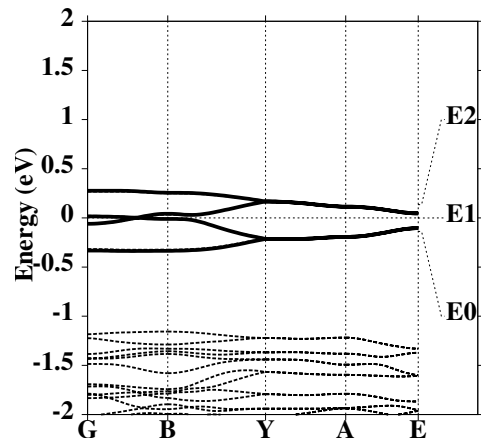


FIG. 5: Bands obtained with downfolded Cu- $d_{x^2-y^2}$ basis (solid lines) compared to full LDA band structure (dashed lines). E_0 , E_1 and E_2 mark the energy points used in NMTO calculation.

ing to the low-energy bands. The real space representation of the downfolded Hamiltonian $H = \sum t_{ij}(c_i^\dagger c_j + h.c)$ in the Wannier function basis gives the various hopping integrals t_{ij} between the effective orbitals.

For the present compound we have derived the low energy Hamiltonian defined in the basis of the effective Cu- $d_{x^2-y^2}$ orbitals, by keeping only the $d_{x^2-y^2}$ orbital for each Cu atom in the unit cell and integrating out all the rest. We show the downfolded bands in Fig. 5 in comparison to the full LDA band structure. With the choice of three energy points E_0 , E_1 and E_2 , downfolded bands are indistinguishable from the Cu- $d_{x^2-y^2}$ dominated bands of the full LDA calculation.

The corresponding Wannier function is plotted in

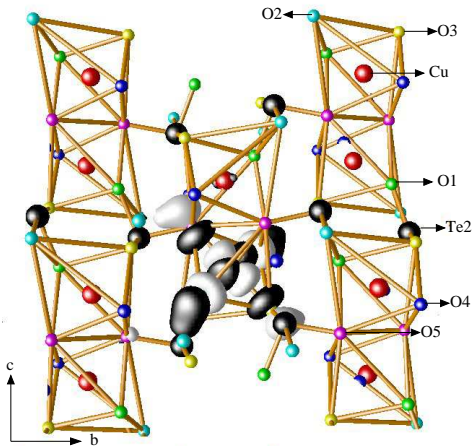


FIG. 6: (Color online) Effective $\text{Cu}d_{x^2-y^2}$ orbital with lobes of opposite signs colored as black and white. The $d_{x^2-y^2}$ orbital is defined with the choice of local reference frame as described in the text.

Fig. 6. The central part has the $3d_{x^2-y^2}$ symmetry with the choice of the local coordinate system as stated above, while the tails are shaped according to $\text{O}-p_x/p_y$. The $\text{Cu}-d_{x^2-y^2}$ orbital forms strong $\text{pd}\sigma$ antibonds with the $\text{O}-p_x/p_y$ tails. $\text{O}-p_x/p_y$ tails bend towards the Te2 atom, what indicates the importance of hybridization effects from the Te cations and enhances the Cu-Cu interaction placed at different structural dimers Cu_2O_{10} .

Table-I shows the various dominant effective hopping integrals t_{ij} with magnitude greater than 1 meV between the $\text{Cu}(\text{II})$ ions at sites i and j . The notation for the various hoppings is shown in Fig. 7 where the subindex of t_n corresponds to the n^{th} Cu neighbors. The strongest hopping integral, t_4 , is found to be between those two $\text{Cu}(\text{II})$ ions which are placed at different structural dimers and the interaction is mediated by two O-Te-O bridges. t_1 , which denotes the hopping integral between two $\text{Cu}(\text{II})$ ions situated within the same structural dimer unit, is found to be about 1/3 of the strongest hopping integral (t_4). The second strongest hopping term, t_6 , mediated by one O-Te-O bridge is about 1/2 of t_4 . Fig. 7b shows the interaction paths in the ab plane, which are weak in general and can be neglected. In particular, we mention as examples the hopping integrals t_3 and t_7 , which are approximately 1/10 and 1/25 of the strongest hopping term (t_4) respectively. In the following we discuss the origin of the various dominant interaction paths.

A. Strongest hopping term $-t_4$

The strongest hopping term, t_4 , mediated by two O-Te-O bridges is associated to a Cu-O-Te-O-Cu super-superexchange (SSE) path generating the spin-spin coupling J_4 . The strength of a SSE interaction through an exchange path of type Cu-O-L-O-Cu (e.g., L=Te) depends sensitively on how the O-L-O linkage orients the

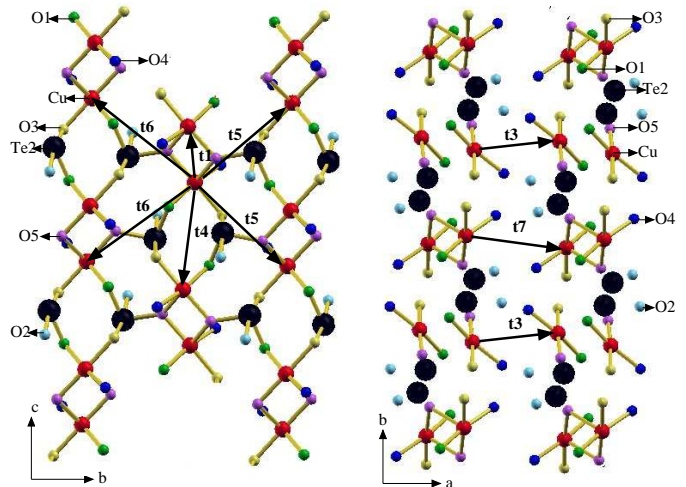


FIG. 7: (Color online) Cu-Cu interaction paths t_n . The color convention is the same as Fig. 2.

TABLE I: Cu-Cu hopping parameters corresponding to the downfolded $\text{Cu}-d_{x^2-y^2}$ Hamiltonian in NMTO-Wannier function basis. Only hopping integrals of strength larger than 1meV are listed.

hopping	Cu-Cu distances	Hopping parameters
	in Å	in meV
t_1	3.18	38.7
t_3	5.32	11.0
t_4	5.58	112.9
t_5	5.83	13.7
t_6	6.20	59.9
t_7	6.43	4.9

two magnetic orbitals (i.e the $d_{x^2-y^2}$ orbitals) centered at two Cu sites and also on how the tails of the magnetic orbitals, which have contributions of the orbitals of the ligand atom L, are oriented with respect to the central part. In Fig. 8 we show the Wannier function plot corresponding to t_4 , where the effective $\text{Cu}-d_{x^2-y^2}$ -like Wannier orbitals are at the Cu sites between which we have found the strongest interaction. The $\text{O}-p_x/p_y$ tails bend towards the Te atoms forming O-Te-O ligand paths which are responsible for the strong Cu-Cu bonding.

B. Second strongest hopping term $-t_6$

The hopping integral t_6 describes the next strong Cu-Cu interaction path, which is mediated via one O-Te-O bridge and responsible for the Cu-O-Te-O-Cu SSE interaction generating the spin-spin coupling J_6 . Fig. 9 shows the Wannier plots of the $\text{Cu}-d_{x^2-y^2}$ downfolded NMTOs. Here the oxygen tails bend towards the inter-connecting TeO_2 unit to provide an interaction pathway between the two Cu sites as in the t_4 path. However the strength of this interaction is expected to be weaker

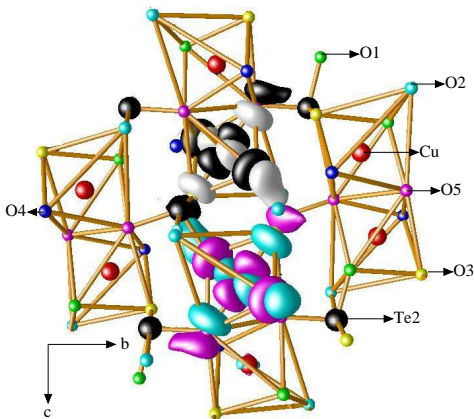


FIG. 8: (Color online) Effective orbital corresponding to the downfolded NMTOs, placed at two Cu sites situated at two different structural dimer units corresponding to the t_4 interaction. Lobes of orbitals placed at different Cu sites are colored differently. Lobe colored black (white) at one Cu site represents the same sign as that colored magenta (cyan) at other Cu site.

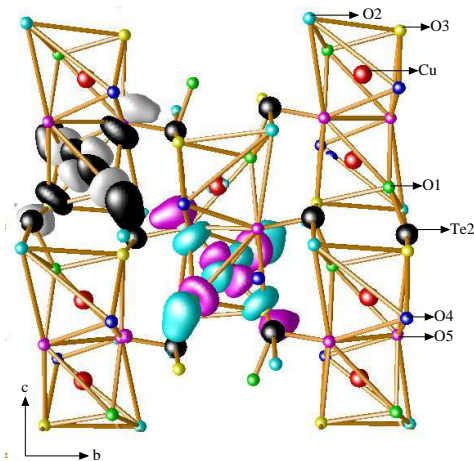


FIG. 9: (Color online) Effective orbital corresponding to the downfolded NMTOs, placed at two Cu sites situated at two different structural dimer units corresponding to the t_6 hopping term. Color convention is same as in Fig. 8.

than t_4 since there is only one, instead of two O-Te-O interaction paths.

C. Structural intradimer hopping term- t_1

t_1 corresponds to the intradimer Cu-Cu interaction path which is mediated by O5-O5' atoms. In Fig. 10 we show the Wannier function plot, where the effective $\text{Cu-d}_{x^2-y^2}$ like Wannier orbitals are placed at the Cu sites of the same structural dimer unit. As we stated above, each structural dimer unit is made of two edge sharing CuO_6 distorted octahedra. In the case of the first octahedron O5 is situated on the basal plane of the octahedron

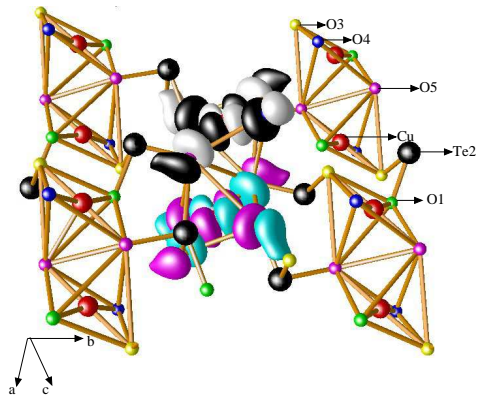


FIG. 10: (Color online) $\text{Cu-d}_{x^2-y^2}$ downfolded NMTOs, placed at two Cu sites situated within same structural dimer. The O2 sites with long Cu-O2 bond lengths have been removed for better view. Color convention is same as in Fig. 8.

and O5- p_x/p_y form $\text{pd}\sigma$ antibond with the $\text{Cu-d}_{x^2-y^2}$ orbital, whereas O5' is situated at the apical position for this octahedron. The reverse is true for the second octahedron. Therefore $\text{Cu-d}_{x^2-y^2}$ orbitals of two Cu^{2+} sites placed at the same structural dimer unit are misaligned, what is responsible for the weak Cu-Cu intradimer interaction. As the Cu-O5-Cu and Cu-O5'-Cu angles turn out to be 96.76 degree, the Cu-Cu interaction within the structural dimer, which is weak in general, is in the borderline where a sign change of exchange interaction from antiferromagnetic to ferromagnetic may occur¹⁵.

V. SUSCEPTIBILITY, MAGNETIZATION AND SPECIFIC HEAT

The description of the spin model for CuTe_2O_5 as obtained from the NMTO-downfolding technique turns out to be that of a system of coupled dimers in a two dimensional (2D) grid (see Fig. 11). In order to check the goodness of our proposed model, we have calculated the magnetic susceptibility as well as magnetization and specific heat properties by considering the following spin-1/2 Heisenberg model on a $N_1 \times N_2$ lattice:

$$\begin{aligned}
 H = & J_1 \sum_{j=0}^{N_2-1} \sum_{i=0}^{\frac{N_1}{2}-1} (\mathbf{S}_{2i,j} \mathbf{S}_{2i+1,j}) + J_4 \sum_{j=0}^{N_2-1} \sum_{i=0}^{\frac{N_1}{2}-1} (\mathbf{S}_{2i+1,j} \mathbf{S}_{2i+2,j}) \\
 & + J_6 \sum_{j=0}^{\frac{N_2}{2}-1} \sum_{i=0}^{\frac{N_1}{2}-1} [(\mathbf{S}_{2i,2j} \mathbf{S}_{2i,2j+1} + \mathbf{S}_{2i,2j} \mathbf{S}_{2i+2,2j+1}) \\
 & + (\mathbf{S}_{2i+1,2j} \mathbf{S}_{2i+1,2j-1} + \mathbf{S}_{2i+1,2j} \mathbf{S}_{2i+3,2j-1})] \quad (1)
 \end{aligned}$$

where J_1 , J_4 and J_6 are the exchange integrals corresponding to the hopping paths t_1 , t_4 and t_6 respectively. Interestingly, this model reduces to the model grid that describes the magnetic behavior of $\text{CaCuGe}_2\text{O}_6$ when $J_1 = 0$. In that case, the two dimensional model

has (using the present notation), two critical points at $J_6 \approx -0.9J_4$ and $J_6 \approx 0.55J_4^4$.

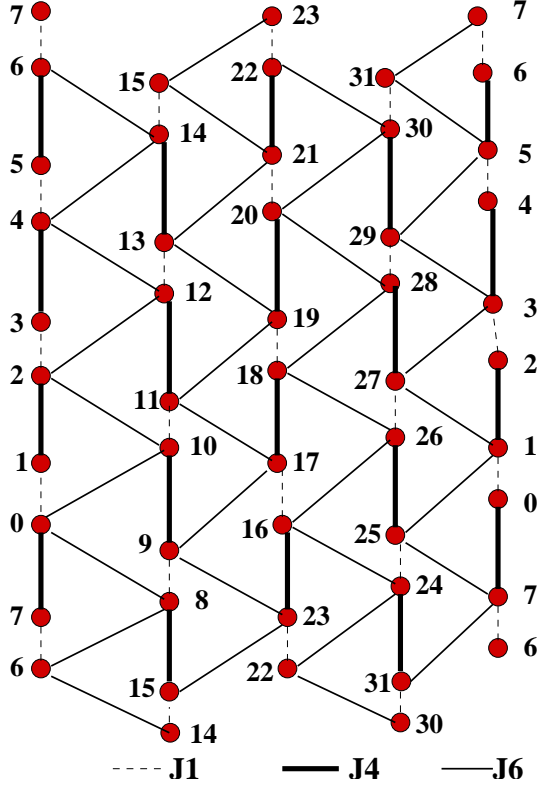


FIG. 11: The 2D coupled dimer model shown on a 8×4 (32 site) lattice. Periodic boundary conditions have been applied on both directions. The thick, thin and dashed lines represent the strongest J_4 , the next strong J_6 and the weak structural intra-dimer interaction J_1 respectively. The site index k is given by $k = N_1 * l + m$, where m runs over number of rows in the square lattice ($m = 0, 1, \dots, N_1$), and l runs over the number of columns in the square lattice ($l = 0, 1, \dots, N_2$).

The analysis of model Eq. 1 has been done by the Quantum Monte Carlo method (stochastic series expansion^{8,9,10}) on a 20×20 lattice. While the NMTO downfolding technique gives us an estimation for hopping parameters, it does not provide directly values of exchange integrals. The exchange coupling, J , can be expressed in general as a sum of antiferromagnetic and ferromagnetic contributions $J = J^{AFM} + J^{FM}$. In the limit of large correlation, typically valid for Cu based system, the antiferromagnetic contribution, J^{AFM} , is related to the hopping integral t by the second order perturbation relation $J^{AFM} = 4t^2/U$, where U is the effective on-site Coulomb repulsion. In absence of a satisfactory approach for computing J directly, in the following we considered the NMTO downfolding inputs to built up the model and starting point for relative estimates of various exchange interactions. We define the parameters,

$$\alpha_1 = \frac{J_6}{J_4}, \quad \alpha_2 = \frac{J_1}{J_4} \quad (2)$$

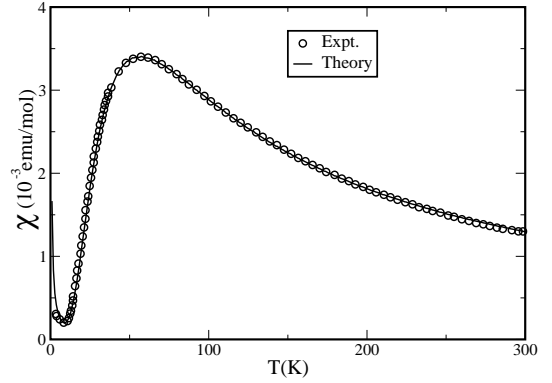


FIG. 12: Temperature dependence of magnetic susceptibility for CuTe_2O_5 . The circles corresponds to experimental data² and the solid line correspond to calculated susceptibility based on a 2D-coupled dimer model.

which measure the ratio of the inter-dimer J_6 and structural intra-dimer J_1 interactions with respect to the exchange interaction which was suggested from the downfolding calculations to be the strongest J_4 .

The optimal values of α_1 and α_2 as well as the strength of the primary interaction J_4 and the effective g factor are obtained by fitting the QMC results for the susceptibility:

$$\chi^{th} = \langle (S^z - \langle S^z \rangle)^2 \rangle \quad (3)$$

(μ_B and k_B denote the Bohr magneton and the Boltzmann constant respectively) with the experimental susceptibility (in [emu/mol]) at intermediate to high temperatures via¹⁴ $\chi = 0.375(g^2/J)\chi^{th}$. To simulate the low temperature region of the susceptibility data we include the respective Curie contribution from impurities as $\chi^{CW} = C_{imp}/T$. The calculated susceptibility in comparison to experimental data is shown in Fig.12.

The best fit corresponds to the intra-dimer exchange integral $J_4 = 92.4$ K, very close to the value proposed by J. Deisenhofer *et al*² for the strongest dimer coupling. The optimal value of the g factor = 2.17 was found to be slightly larger than the spin only value of $g=2$, in agreement with ESR measurement. The optimal values for the coupling ratios in Eq. 2 are found to be $\alpha_1 = 0.27$ and $\alpha_2 = 0.07$, rather close to the estimates, 0.28 and 0.11 respectively, obtained using the second-order perturbation relationship between exchange interaction (J) and the hopping integral (t) given by the NMTO-downfolding study. The weak J_1 interaction turned out to be of antiferromagnetic nature giving rise to a positive sign for α_2 . With the stochastic series expansion implementation of the quantum Monte Carlo method it is possible to simulate quantum spin models in an external field. In Fig. 13, we present the computed magnetization as a function of temperature $M(T)$ for various magnetic fields' strengths and in Fig. 14 we show the comparison of $M(T)$ for the model proposed in this work and the alternating chain model of Deisenhofer *et al*.² for $H = 12.7$ Teslas and

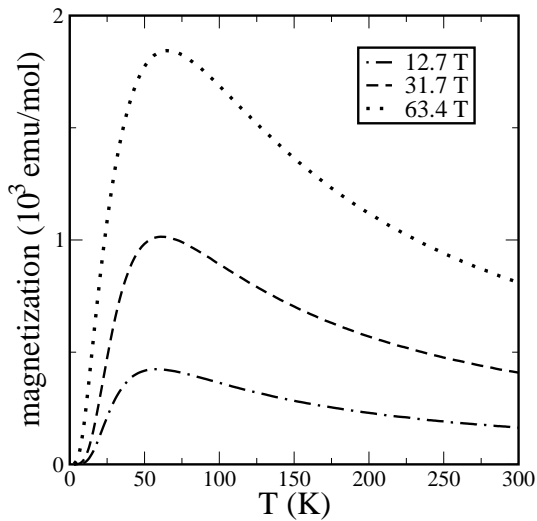


FIG. 13: Magnetization plotted as a function of temperature for the 2D-coupled dimer model of CuTe_2O_5 in an applied magnetic field of strengths $h/J=0.2, 0.5, 1.0$ (bottom to top) which correspond to $H = 12.7, 31.7, 63.4$ Teslas.

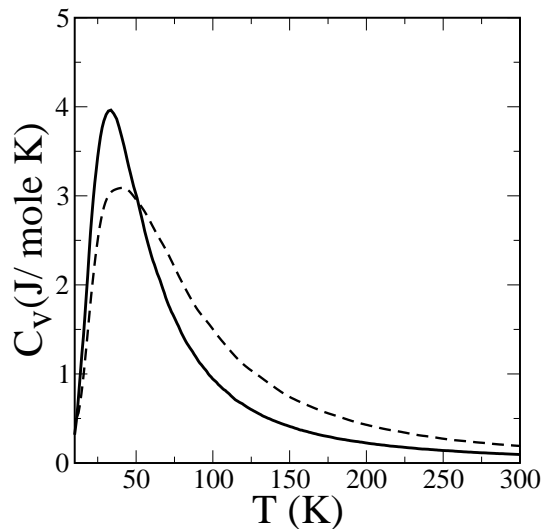


FIG. 15: Specific heat plotted as a function of temperature for CuTe_2O_5 for the 2D-coupled dimer model (solid line) and the model of Ref. 2 (dashed line).

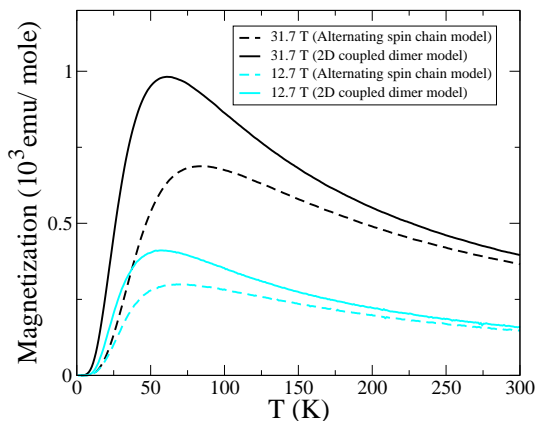


FIG. 14: (Color online) Magnetization plotted as a function of temperature for the 2D-coupled dimer model of CuTe_2O_5 and the alternating chain model of Ref. 2 for two values of the magnetic field $H = 12.7$ Teslas and $H = 31.7$ Teslas.

$H = 31.7$ Teslas. Two models show distinctly different behavior at moderate to high magnetic fields.

We also calculated the specific heat $C_v(T)$ for both models and the results are presented in Fig. 15. While the overall qualitative shapes of the $C_v(T)$ versus temperature curves for both models are similar, there are important quantitative distinctions which capture the different nature of the models.

Our above computed thermodynamic quantities provide a useful framework to test the validity of our proposed model in terms of further experimental measurements.

VI. CONCLUSION

The analysis of the electronic structure of CuTe_2O_5 by first-principles NMTO-downfolding calculations as well as the calculation and examination of susceptibility data by the QMC method leads to a unique description of this system as a 2D coupled dimer model. The strongest Cu-Cu interaction is between Cu pairs belonging to different structural dimer units and connected by two O-Te-O bridges. Two additional in-plane interactions of about $1/3$ and $1/10$ of the strongest interaction have been found; the latter one being the structural intra-dimer interaction. This is in disagreement with recent theoretical considerations in Ref. 2, which suggest the CuTe_2O_5 system as an alternating spin chain system with strong intra- and inter-dimer coupling. Based on our proposed model, we have also calculated the magnetization and specific heat which may be compared with new experimental measurements. We hope that our work will stimulate further experimental studies.

VII. ACKNOWLEDGMENT

We would like to thank P. Lemmens and J. Deisenhofer for discussions and for bringing the problem into our attention. HD and TSD acknowledge MPG-India partner group program for the collaboration. C.G. and R.V thank the German Science Foundation (DFG) for financial support through the TRR/SFB 49 program.

-
- ¹ P. Lemmens, G. Guntherodt, and C. Gros, *Phys.Rep.* **375**, 1 (2003).
- ² J. Deisenhofer et.al. *Phys.Rev.B* **74**, 174421 (2006).
- ³ O. K. Andersen and T. Saha-Dasgupta, *Phys. Rev. B* **62**, R16219 (2000).
- ⁴ R. Valentí, T. Saha-Dasgupta, and C. Gros, *Phys. Rev. B* **66**, 054426 (2002).
- ⁵ S. Derakhshan, H. L. Cuthbert, J. E. Greedan, B. Raha-
man, and T. Saha-Dasgupta, *Phys. Rev. B* **76**, 104403
(2007); R. Valentí, T. Saha-Dasgupta, C. Gros, and H.
Rosner, *Phys. Rev. B* **67**, 174405 (2003).
- ⁶ T. Saha-Dasgupta, R. Valentí, F. Capraro, and C. Gros
Phys. Rev. Lett. **95**, 107201 (2005); R. Valentí and T.
Saha-Dasgupta *Phys. Rev. B* **65**, 144445 (2002); R. Val-
entí, T. Saha-Dasgupta, J. V. Alvarez, K. Pozgajcic, and
C. Gros *Phys. Rev. Lett.* **86**, 5381 (2001).
- ⁷ P. Lemmens, K.Y. Choi, R. Valentí, T. Saha-Dasgupta, E.
Abel, Y.S. Lee, and F.C. Chou *New J. Phys.* **7**, 74 (2005);
T. Saha-Dasgupta, R. Valentí, H. Rosner, and Claudius
Gros *Europhys. Lett.* **67**, 63 (2004).
- ⁸ A.W. Sandvik, *Phys. Rev. B* **59**, R14157 (1999).
- ⁹ A. Dorneich and M. Troyer, *Phys. Rev. E* **64**, 066701
(2001).
- ¹⁰ K. Louis and C. Gros, *Phys. Rev. B* **70**, R100410 (2004).
- ¹¹ K. Hanke, V. Kupcik, O. Lindqvist, *Acta Cryst. B* **29**, 963
(1973).
- ¹² P. Blaha, K. Schwarz, G. K. H. Madsen, D. Kvasnicka, and
J. Luitz, computer code WIEN2K, 2001.
- ¹³ O. K. Andersen, *Phys. Rev. B*, **12**, 3060 (1975).
- ¹⁴ D. C. Johnston, R. K. Kremer, M. Troyer, X. Wang, A.
Klümper, S. L. Bud'ko, A. F. Panchula, and P. C. Canfield,
Phys. Rev. B **61**, 9558 (2000).
- ¹⁵ J. B. Goodenough, *Phys. Rev.* **100**, 564 (1955); J.
Kanamori, *J. Phys. Chem. Solids* **10**, 87 (1959); P.W. An-
derson, *Solid State Phys.* **14**, 99 (1963).